AGU PUBLICATIONS

Water Resources Research

RESEARCH ARTICLE
10.1002/2015WR017504

Key Points:
- Variability of the Priesley-Taylor coefficient over water bodies is explained
- A new method for estimating the Priesley-Taylor coefficient is proposed
- The new method can be applied to standard meteorological sensors

Correspondence to:
D. Li,
danl@princeton.edu

Citation:
Assouline, S., D. Li, S. Tyler, J. Tanny, S. Cohen, E. Bou-Zeid, M. Parlange, and G. G. Katul (2016), On the variability of the Priestley-Taylor coefficient over water bodies, *Water Resour. Res.*, *52*, 150–163, doi:10.1002/2015WR017504.

Received 5 MAY 2015
Accepted 18 NOV 2015
Accepted article online 9 DEC 2015
Published online 11 JAN 2016

On the variability of the Priestley-Taylor coefficient over water bodies

Shmuel Assouline[1], Dan Li[2], Scott Tyler[3], Josef Tanny[1], Shabtai Cohen[1], Elie Bou-Zeid[4], Marc Parlange[5], and Gabriel G. Katul[6]

[1]Institute of Soil, Water and Environmental Sciences, Agricultural Research Organization, Volcani Center, Bet Dagan, Israel, [2]Program of Atmospheric and Oceanic Sciences, Princeton University, Princeton, New Jersey, USA, [3]Department of Geological Sciences and Engineering, University of Nevada, Reno, Nevada, USA, [4]Department of Civil and Environmental Engineering, Princeton University, Princeton, New Jersey, USA, [5]Department of Civil Engineering, University of British Columbia, Vancouver, British Columbia, Canada, [6]Nicholas School of the Environment, Duke University, Durham, North Carolina, USA

Abstract Deviations in the Priestley-Taylor (PT) coefficient α_{PT} from its accepted 1.26 value are analyzed over large lakes, reservoirs, and wetlands where stomatal or soil controls are minimal or absent. The data sets feature wide variations in water body sizes and climatic conditions. Neither surface temperature nor sensible heat flux variations alone, which proved successful in characterizing α_{PT} variations over some crops, explain measured deviations in α_{PT} over water. It is shown that the relative transport efficiency of turbulent heat and water vapor is key to explaining variations in α_{PT} over water surfaces, thereby offering a new perspective over the concept of minimal advection or entrainment introduced by PT. Methods that allow the determination of α_{PT} based on low-frequency sampling (i.e., 0.1 Hz) are then developed and tested, which are usable with standard meteorological sensors that filter some but not all turbulent fluctuations. Using approximations to the *Gram* determinant inequality, the relative transport efficiency is derived as a function of the correlation coefficient between temperature and water vapor concentration fluctuations (R_{Tq}). The proposed approach reasonably explains the measured deviations from the conventional $\alpha_{PT} = 1.26$ value even when R_{Tq} is determined from air temperature and water vapor concentration time series that are Gaussian-filtered and subsampled to a cutoff frequency of 0.1 Hz. Because over water bodies, R_{Tq} deviations from unity are often associated with advection and/or entrainment, linkages between α_{PT} and R_{Tq} offer both a diagnostic approach to assess their significance and a prognostic approach to correct the 1.26 value when using routine meteorological measurements of temperature and humidity.

1. Introduction

The Priestley-Taylor (PT) equation [*Priestley and Taylor*, 1972], presumed to represent wet-surface evaporation from large areas under minimal advective conditions, remains the work-horse model in a myriad of hydrological applications [*Szilagyi et al*., 2014; *Szilagyi*, 2014; *Szilagyi and Schepers*, 2014; *Szilagyi et al*., 2009; *Szilagyi and Jozsa*, 2008; *Crago and Crowley*, 2005; *Pereira*, 2004; *Lhomme*, 1997; *Crago*, 1996; *Eichinger et al*., 1996; *Chen and Brutsaert*, 1995; *Culf*, 1994; *Parlange and Katul*, 1992a; *Viswanadham et al*., 1991; *Granger*, 1989; *Granger and Gray*, 1989; *De Bruin*, 1983; *Spittlehouse and Black*, 1981; *De Bruin and Keijman*, 1979; *Brutsaert and Stricker*, 1979]. It is often used as the wet-surface evaporation reference in complementary models or "advection-aridity" approaches relating actual to potential evaporation [*Brutsaert and Stricker*, 1979; *Granger*, 1989; *Granger and Gray*, 1989; *Parlange and Katul*, 1992a; *Venturini et al*., 2008]. It has been used to define and quantify the coupling coefficient between vegetation and the atmosphere [*Jarvis and McNaughton*, 1986; *McNaughton and Jarvis*, 1991; *Pereira*, 2004]. The PT equation even out performed several detailed models when predicting evaporation from mountainous regions [*Nullet and Giambelluca*, 1990] and semiarid rangelands [*Stannard*, 1993]. It is now routinely employed in estimates of dry-canopy evaporation over forested systems [*Komatsu*, 2005]. It is the preferred formulation for quantifying evaporation from large water bodies in a number of weather-forecasting systems [*Yu*, 1977] including the European Center for Medium-Range Weather Forecasts [*Szilagyi et al*., 2014].

The only empirical parameter in the PT formulation is α_{PT}, the well-known Priestley-Taylor coefficient whose value was determined to be $\alpha_{PT} \approx 1.26$ using daily measurements of evapotranspiration. A number of

subsequent studies and theories confirmed a near-constant $\alpha_{PT} \in [1.2, 1.3]$ [*Parlange and Katul*, 1992b; *Eichinger et al*., 1996; *Lhomme*, 1997; *Brutsaert*, 2005; *De Bruin*, 1983; *Wang et al*., 2004]. This near constancy in α_{PT} proved to be attractive when up-scaling remote sensing data given the direct link between α_{PT} and the evaporative fraction [*Crago*, 1996]. However, many studies have reported large variations in α_{PT} and deviations from its accepted 1.26 value that cannot be explained by measurement errors alone, especially at subdaily time scales. For example, *De Bruin and Keijman* [1979] found α_{PT} values as high as 1.5 and as low as 1.2 depending on the season. Similar seasonal variability in the 1.1–1.4 range was reported for α_{PT} in a region dominated by the Asian monsoon [*Yang et al*., 2013]. One study suggested correlations between α_{PT} and pasture leaf area index variability [*Sumner and Jacobs*, 2005]. For moist tropical forests, *Viswanadham et al*. [1991] reported α_{PT} to vary from 0.67 to 3.12 depending on thermal stratification (i.e., α_{PT} is connected to the buoyant production or destruction of turbulent kinetic energy, which in turn, is linked to sensible heat flux H). In partial support of this argument, *Pereira and Villa-Nova* [1992] showed that α_{PT} increases with increasing H based on lysimeter data collected in well-irrigated crops. The α_{PT} was also reported to depend on water content of drying soil surfaces, reaching values as low as 0.25 for relatively dry soil surfaces [*Davis and Allen*, 1973; *Flint and Childs*, 1991; *Aminzadeh and Or*, 2014]. *Cho et al*. [2012] analyzed data from 25 *FLUXNET* sites and reported variations in α_{PT} between 0.01 and 1.53, though these values were then correlated to a normalized surface resistance. A recent study by *Guo et al*. [2015] analyzed 30 min flux data collected over saturated water and glacier surfaces. They separated the data into three regimes according to the direction of sensible (H) and latent heat (E) fluxes (regime I: $H > 0$; $E > 0$, regime II: $H < 0$; $E > 0$, regime III: $H < 0$; $E < 0$) and found that the variations of α_{PT} are significantly different among the three regimes. Over water surfaces, α_{PT} was reported to be within the ranges of 1.00–1.32 and 1.24–2.04 for regimes I and II, respectively; over glacier surfaces, $\alpha_{PT} < -0.10$ or $\alpha_{PT} > 1.70$ in regime II and $0.08 < \alpha_{PT} < 1.0$ in regime III. This highlights the importance of Bowen ratio in modulating variations in α_{PT}. Other processes such as advection [*Jury and Tanner*, 1975] and the behavior of the convective boundary layer [*McNaughton and Spriggs*, 1986; *Monteith*, 1995; *Huntingford and Monteith*, 1998] have been also shown to affect α_{PT}. Explaining the causes of all these variations in α_{PT} partly motivates the work here.

As a starting point, the main objective here is to explore what governs variations in α_{PT} at subdaily time scales over large water bodies, where soil or stomatal controls are absent or minimal. The sites include Lake Léman in Switzerland and Lake Kinneret in Israel, the settling and the operational reservoirs at Eshkol, Israel, and the Tilopozo wetland of the Atacama Desert in Chile, featuring wide variations in sizes and climatic conditions. H and E fluxes and micrometeorological data were collected at all these sites. It is shown that the relative transport efficiency of heat and water vapor R_{Tq} is the key to explaining observed variability in α_{PT}. Given the links between R_{Tq} and processes such as advection, entrainment, and dissimilarity in sources and sinks of heat and water vapor at the water surface, the method developed here also offers a novel diagnostic framework to assess their significance on α_{PT}. Building on the connection between α_{PT} and R_{Tq}, a corollary objective is to propose a prognostic method that allows the determination of α_{PT} from R_{Tq} on short (e.g., diurnal) time scales, where the latter may be inferred from standard meteorological sensors that filter some (but not all) turbulent fluctuations. The proposed method also does not require any vertical velocity time series information and operates reasonably on simultaneously sampled but filtered air temperature and atmospheric water vapor concentration series even when the sensor cutoff frequency is as low as 0.1 Hz (typical for thermocouples and electric capacitive hygrometers used in standard weather stations).

2. Data Sets

Because some approximations in the theoretical development employ the data sets, they are presented first. The flux data were obtained by the eddy covariance (EC) method supplemented by additional micrometeorological variables including air (T_a) and surface (T_s) temperatures. The use of the EC method for estimating H and E over water has a long history that is reviewed elsewhere [*Tanner and Greene*, 1989; *Stannard and Rosenberry*, 1991; *Assouline and Mahrer*, 1993; *Bates et al*., 1995; *Blanken et al*., 2000, 2003; *Panin et al*., 2006; *Tanny et al*., 2008; *Jonsson et al*., 2008; *Rouse et al*., 2008; *Liu et al*., 2009; *Blanken et al*., 2011; *Granger and Hedstrom*, 2011; *Tanny et al*., 2011; *Nordbo et al*., 2011]. The data sets used here correspond to different water bodies of different sizes, geographic locations, and climates. These sites include Lake Léman and Lake Kinneret, a settling and an operational reservoir at Eshkol, and the Tilopozo wetland in an arid environment.

Briefly, Lake Léman (also known as Lake Geneva; 46°26′N 6°33′E; 372 m.a.s.l.) is the largest lake in Switzerland (580 km^2) located at the border between Switzerland (from the north, east, and west) and France (from the south). It is part of the Rhone River that starts in the Alps and eventually flows into the Mediterranean Sea. The climate around the lake is temperate. The measurements were collected on a 10 m high tower (although the sensors used here were below 4 m), 100 m away from the northern shore of the lake during the late summer and autumn of 2006 [*Assouline et al*., 2008; *Bou-Zeid et al*., 2008; *Vercauteren et al*., 2008; *Li and Bou-Zeid*, 2011; *Li et al*., 2012a, 2012b]. Sampling frequency and averaging intervals were 20 Hz and 30 min, respectively, as described elsewhere [*Li et al*., 2015]. Only data with wind coming from the south and southwest were used to ensure that the tower did not influence the measurements and that the minimum fetch was 10 km [*Vercauteren et al*., 2008]. Because of the high sampling rate and extensive fetch, data from this site are used for illustration and case studies.

Lake Kinneret (also known as the Sea of Galilee; 32°50′N 35°35′E; −212 m.a.s.l.) is situated in the upper Galilee (northeastern Israel), in the central part of the Jordan Rift Valley. It has an area of 166 km^2 and a semiarid climate. Measurements were carried out at 2.0 m above the water surface, 200 m away from the western shore, from May to June and from September to October 1990. Fluxes were sampled at 5 Hz and averaged every 15 min [*Assouline and Mahrer*, 1993].

The Eshkol reservoirs are located in the Bet-Netofa Valley in northern Israel (32°46′N 35°14′E; 145 m.a.s.l), a site characterized by a Mediterranean climate. Two reservoirs in series, settling and operational, are constructed as part of the National Water Carrier system. The settling reservoir is geometrically square in planar area with a 600 m side and a mean depth of 3.5 m (with minor variations). Measurements were conducted at 2.4 m above the water surface using a platform situated at the center of the reservoir during the summer of 2005 [*Tanny et al*., 2008; *Assouline et al*., 2008]. Water flows out of this reservoir into the adjacent operational reservoir, twice as large as the settling reservoir in terms of area, with water level fluctuations resulting from daily and weekly cycles of operation. Measurements from a station above the water of the operational reservoir were conducted during the summer of 2008 [*Tanny et al*., 2011]. Due to water level variations, sensor height above the water surface varied between 1.4 and 4.7 m. In both cases, sampling frequency and averaging intervals were 10 Hz and 15 min, respectively.

The Tilopozo wetland is located in the hyperarid Atacama Desert in northern Chile at the southern end of the Salar de Atacama (23°47′S 68°14′W; 2320 m.a.s.l.). It consists of a complex of springs, ponds, wetlands, and phreatophyte vegetation within an area of approximately 600 ha. The climate of the region can be considered hyperarid. Measurements at 2 m above the surface from a station installed in the central portion of the Tilopozo wetland (flooded wetland vegetation in a saturated soil situation) were carried out during the winter of 2002 [*Assouline et al*., 2008]. In this case, sampling frequency and averaging intervals were 10 Hz and 15 min, respectively.

3. Theory

3.1. Background and General Definitions

As a starting point for quantifying the causes of α_{PT} variations, the one-dimensional energy budget at the water-atmosphere interface is considered and is given by

$$R_n - E - H - G = 0, \tag{1}$$

where R_n is the net radiation and G is the heat flux into the water at the air-water interface. Even when R_n and G are measured or indirectly determined, equation (1) cannot be used in practice to determine E because H is unknown. However, it can be employed to infer bounds on α_{PT} when used in conjunction with the Penman equation [*Penman*, 1948] that is applicable to wet surfaces and is given by

$$E_{PE} = \frac{\Delta}{\Delta+\gamma}(R_n - G) + \frac{\gamma}{\Delta+\gamma}E_A, \tag{2}$$

where E_A is an atmospheric drying function that represents the capacity of the atmosphere to transport water vapor and can vary with the thermal stratification in the atmosphere [*Brutsaert*, 2005; *Katul and Parlange*, 1992], Δ (Pa K^{-1}) is the rate of increase of saturation vapor pressure with increasing temperature, and γ is the psychrometric constant, respectively, defined as:

$$\Delta=\frac{d\,e^*}{d\,T}\Big|_{T_s}\approx\frac{(e_s^*-e_a^*)}{(T_s-T_a)};\;\;\gamma=\frac{c_p\,p}{0.622\,L_e}, \tag{3}$$

where e_s^* and e_a^* denote saturation vapor pressures (in Pa) at the water surface temperature T_s and atmospheric air temperature T_a, respectively, p denotes atmospheric pressure (in Pa), c_p (J kg^{-1} K^{-1}) and L_e (J kg^{-1}) are the specific heat capacity of dry air at constant pressure and the latent heat of vaporization of water, respectively. In practice, γ and Δ can be approximated from T_s (in units of °C) using the following expressions based on data in *Brutsaert* [2005]:

$$\Delta=63.40\exp\left(\frac{T_s}{21.35}\right)-17.23;\;\;\gamma=\frac{c_p\,p}{0.622\,(2501.2-2.4\,T_s)}. \tag{4}$$

PT determined the bounding limits on α_{PT} as follows. When $E_A=0$ in equation (2), a lower limit on E can be derived from E_{PE} over an extensive water surface. This rate is the so-called equilibrium latent heat flux, $E_e=\frac{\Delta}{\Delta+\gamma}(R_n-G)$, and can be used to define $\alpha_{PT}=E/E_e$ [*Slatyer and McIlroy*, 1967; *Monteith*, 1981]. It follows that when $E=E_e$, $\alpha_{PT}=1$, which is the lower limit on α_{PT} proposed by PT. As an upper limit on E, an $H=0$ was set by PT so that the maximum $E=R_n-G$ from energy balance considerations alone. PT associated conditions where $H<0$ to be "advection," where extra energy becomes available to E beyond the upper limit set by R_n-G. Using the definition $\alpha_{PT}=E/E_e$, and in the absence of "advection" (i.e., $H<0$), it follows that $1<\alpha_{PT}<(\Delta+\gamma)/\Delta$. The upper limit is set by the fact that $(R_n-G)/E_e=(R_n-G)/[(\Delta/(\Delta+\gamma))(R_n-G)]=(\Delta+\gamma)/\Delta$. The upper limit $(\Delta+\gamma)/\Delta$ decreases with increasing temperature from roughly 2.4 at 0°C to 1.17 at 40°C. Based on daily data obtained over oceans and moist land surfaces, PT found that α_{PT} is reasonably constant (about 1.26). Later studies supported $\alpha_{PT}=1.26$ by other theoretical considerations [*Eichinger et al.*, 1996; *Lhomme*, 1997; *Wang et al.*, 2004]. It is commonly assumed that for moist surfaces, $1.2<\alpha_{PT}<1.3$ [*Brutsaert*, 2005].

3.2. Variations of α_{PT} With Surface Temperature

Because the upper limit of α_{PT} (i.e., $(\Delta+\gamma)/\Delta$) decreases with increasing temperature and approaches the lower limit (i.e., unity) for large T_s, a temperature dependency in α_{PT} may be expected. In fact, PT already noted that $\alpha_{PT}=1.26$ roughly coincides with the arithmetic average of the upper and lower bounds for the range of (daily) temperatures considered. Starting from their suggestion, a plausible argument for introducing a temperature correction to α_{PT} is to assume that

$$\alpha_{PT}\approx\alpha_{avg}=\frac{\left(1+\frac{\Delta+\gamma}{\Delta}\right)}{2}. \tag{5}$$

However, accounting for T_s variations to explain α_{PT} deviations from the 1.26 value remains ad hoc and cannot explain subunity or large values (>2) in α_{PT} reported by a number of studies (including the present study, as shown later). To proceed theoretically further, an alternative definition of α_{PT} is preferred that admits a broader range of extremum values.

3.3. Defining α_{PT} Using a Bowen Ratio Form

In the context of equation (1), the α_{PT} can be uniquely related to the Bowen ratio $\beta=H/E$ and T_s using:

$$\alpha_{PT}=\frac{E}{E_e}=\frac{\Delta+\gamma}{\Delta}\frac{E}{(R_n-G)}=\frac{\Delta+\gamma}{\Delta}\frac{1}{(1+\beta)}. \tag{6}$$

Such a *definition* suggests that α_{PT} needs not be bounded by the aforementioned limits set by PT when advective effects are significant. For example, $\alpha_{PT}\to\infty$ when $\beta=-1$ (i.e., when $R_n-G=0$). Also, $\alpha_{PT}\to 0$ as $E\to 0$. From equation (6), it is made clear that α_{PT} is related to $(1+\beta)^{-1}$ and T_s (instead of T_s in isolation as in equation (5)). The product $[\alpha_{PT}(1+\beta)]$ must exceed unity and is a function of T_s solely. For large T_s, Δ becomes large, $(\Delta+\gamma)/\Delta=1+\gamma/\Delta\approx 1$ and $[\alpha_{PT}(1+\beta)]\to 1$ instead of $\alpha_{PT}\to 1$ as originally proposed by PT. As shall be seen later in Figure 2, α_{PT} indeed becomes large at negative β and drops below 1 at large positive β over water surfaces.

It must also be emphasized that equation (6) and equation (5) are based on a different set of assumptions. Equation (6) makes no assumption about E (i.e., the surface needs not be wet and $E\neq E_{PE}$) and simply provides an alternative definition of α_{PT} as a function of the Bowen ratio and surface temperature. On the other hand, equation (5) assumes that the surface is wet and E cannot drop below its equilibrium state E_e and

cannot exceed the available energy dictated by $R_n - G$ (i.e., no advection). Because of these assumptions, equation (5) can be viewed as prognostic. In contrast, equation (6) is only diagnostic in that it shows how variations in α_{PT} relate to β. It cannot be used in a "prognostic" form without some estimate or a model for β, the subject of the next two sections.

3.4. Determining α_{PT} From Flux-Gradient Theory

Consider the Bowen ratio β obtained when relating turbulent fluxes to their mean gradients using [*Brutsaert*, 2005]

$$\beta = \frac{H}{E} = \frac{\rho c_p}{\rho L_e}\frac{K_T}{K_q}\frac{(T_s - T_a)}{(q_s - q_a)}, \tag{7}$$

where K_T and K_q are the turbulent diffusivities for heat and water vapor, respectively, q_s and q_a are the specific humidity (kg kg^{-1}) at the water surface and in the atmosphere, respectively. Denoting $\beta_{ap} = \frac{\rho c_p}{\rho L_e}\frac{(T_s - T_a)}{(q_s - q_a)}$ leads to

$$\frac{\beta}{\beta_{ap}} = \frac{K_T}{K_q}, \tag{8}$$

and suggests a link between the ratio of heat and vapor diffusivities and α_{PT} using

$$\alpha_{PT} = \frac{\Delta + \gamma}{\Delta}\left[\left(\beta_{ap}\frac{K_T}{K_q}\right) + 1\right]^{-1}. \tag{9}$$

Using β_{ap} inferred from measured T_s, T_a, and q_a and measured fluxes (hence measured α_{PT}), K_T/K_q was computed from equation (9) for all the data sets here. This calculation showed that K_T/K_q varied between 0.1 and 1.0 for the lake data (figure not shown for brevity). Hence, with such large uncertainty in K_T/K_q and no clear theoretical tactic to infer this ratio from routine meteorological measurements, the question as to whether variability in α_{pt} can still be determined from such routine meteorological measurements remains open.

3.5. Determining α_{PT} From Flux-Variance Theory

From its definition, β can also be determined from [*Stull*, 1988]

$$\beta = \frac{H}{E} = \frac{\rho c_p \overline{w'T'}}{\rho L_e \overline{w'q'}} = \frac{\rho c_p}{\rho L_e}\frac{\sigma_w}{\sigma_w}\frac{\sigma_T}{\sigma_q}\left(\frac{R_{wT}}{R_{wq}}\right) = \frac{C_p}{L_e}\left(\frac{\sigma_T}{\sigma_q}\right)T_r. \tag{10}$$

Here the overbar indicates Reynolds averaging (e.g., time averaging), and primed quantities are turbulent fluctuations from Reynolds-averaged (e.g., time-averaged) states, T' are air temperature fluctuations (K) around their mean value T_a, and q' are atmospheric specific humidity fluctuations (kg kg^{-1}) around their mean value q_a, w' are vertical velocity fluctuations (m s^{-1}), $\sigma_T^2 = \overline{T'^2}$ and $\sigma_q^2 = \overline{q'^2}$ are the air temperature variance and the atmospheric water vapor concentration variance, respectively, and $\sigma_w^2 = \overline{w'^2}$ is the vertical velocity variance. The R_{wT} and R_{wq} are correlation coefficients between turbulent vertical velocity and turbulent air temperature fluctuations and between turbulent vertical velocity and water vapor concentration fluctuations, respectively. The quantity $T_r = R_{wT}/R_{wq}$ is known as the relative transport efficiency of turbulence. When $|T_r| > 1$, atmospheric turbulence is transporting heat more efficiently when compared to water vapor and conversely when $|T_r| < 1$. No surface temperature measurements are needed in equation (10). In general, σ_T and σ_q may be determined from low-frequency measurements (e.g., 1–0.1 Hz) as variances are typically dominated by large-scale (and thus low frequency) turbulent excursions. Also, high-frequency losses may be modeled and their variance added by assuming inertial subrange scaling applies for all the "missing" frequencies.

However, in analogy to K_T/K_q, T_r also deviates appreciably from unity even above uniform water bodies as discussed elsewhere [*Assouline et al.*, 2008]. If low-frequency measurements of T' and q' can be used to determine T_r, then the approach here can offer a prognostic method to infer α_{PT} from routine meteorological data. As shown next, the degree of correlation between T' and q' may be used to estimate T_r even when T' and q' are sampled at low frequency with some instrument filtering.

Under some conditions, it may be experimentally shown that [*Bink and Meesters*, 1997; *Katul and Hsieh*, 1997, 1999; *Lamaud and Irvine*, 2006]

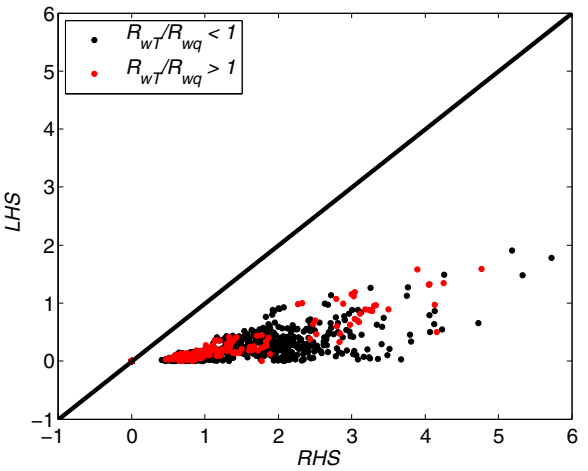

Figure 1. Comparison between the *LHS* and *RHS* of the *Gram* determinant inequality in equation (12) for the 20 Hz data collected above Lake Léman.

$$T_r = \frac{R_{wT}}{R_{wq}} \approx \begin{cases} R_{Tq} \text{ if } R_{wT} < R_{wq} \\ R_{Tq}^{-1} \text{ if } R_{wT} > R_{wq} \end{cases}. \quad (11)$$

A plausibility argument is now provided for this approximation. The general correlation matrix between three arbitrary random variables labeled x, y, and z satisfies the *Gram* determinant inequality given by [*Courant and Hilbert*, 1953]

$$\left| \frac{R_{xy}}{R_{xz}} - R_{yz} \right| \le \frac{1}{R_{xz}} \sqrt{1-R_{xz}^2} \sqrt{1-R_{yz}^2}. \quad (12)$$

An analysis on the relative magnitudes of the left-hand (*LHS*) and right-hand (*RHS*) sides of equation (12) was conducted using the 20 Hz data collected above Lake Léman as a case study and shown in Figure 1. When selecting variables $x = w$, $y = T$, and $z = q$, it was found that across a wide range of atmospheric stability conditions, (i) the *RHS* is always nonzero and is at least an order of magnitude larger than the *LHS* consistent with other studies over land [*Bink and Meesters*, 1997], and (ii) the *LHS* remains small for the majority of the runs analyzed. While the *RHS* appears not to offer significant constraints on the *LHS* as originally envisioned when conducting this analysis, the *LHS* appears to be small independently (at least compared to the *RHS*), which is in agreement with the finding in *Katul and Hsieh* [1997]. Hence, as an approximation of maximum simplicity that ensures that the inequality in equation (12) is always satisfied and yet remains faithful to the empirical evidence of a small *LHS* is to select

$$\left| \frac{R_{xy}}{R_{xz}} - R_{yz} \right| \approx 0, \quad (13)$$

provided $x = w$ and y and z are assigned either as T and q or q and T depending on the quantity $|R_{yz}|$ being ≤ 1 when it is inferred from R_{wy}/R_{wz}. Stated differently, when evaluating R_{Tq} from R_{wy} and R_{wz}, it becomes necessary to select variables y and z such that $R_{wy}/R_{wz} \le 1$. For these conditions, it follows that

$$R_{Tq} \approx \begin{cases} \frac{R_{wT}}{R_{wq}}, \text{ when } R_{wT} < R_{wq} \\ \frac{R_{wq}}{R_{wT}}, \text{ when } R_{wq} < R_{wT} \end{cases}. \quad (14)$$

This implies that

$$\alpha_{PT} \approx \frac{\Delta+\gamma}{\Delta} \left[1 + \frac{C_p}{L_e} \left(\frac{\sigma_T}{\sigma_q} \right) T_r \right]^{-1}, \quad (15)$$

where T_r may be estimated from R_{Tq} or R_{Tq}^{-1}. This α_{PT} estimate does not require any vertical velocity time series information. Its operational utility is based on the assumption that air temperature and water vapor concentration time series collected from thermocouples and electric capacitive hygrometers used in standard weather stations can still be used to infer σ_T/σ_q and R_{Tq}. It is this method and its operational utility that constitutes the main novelty of the work here.

4. Results and Discussion

To illustrate the range in α_{PT} (and β) covered by all the experiments, α_{PT} is first computed from equation (6) using EC measured H and E fluxes and T_s for each site and period. As evident from Figure 2, the data sets span a broad range of α_{PT} and β. From the definition in equation (6), α_{PT} is expected to decrease with increasing β and $\alpha_{PT} = 1.26$ occurs roughly around $\beta = 0$ or slightly negative. The relation between α_{PT} and

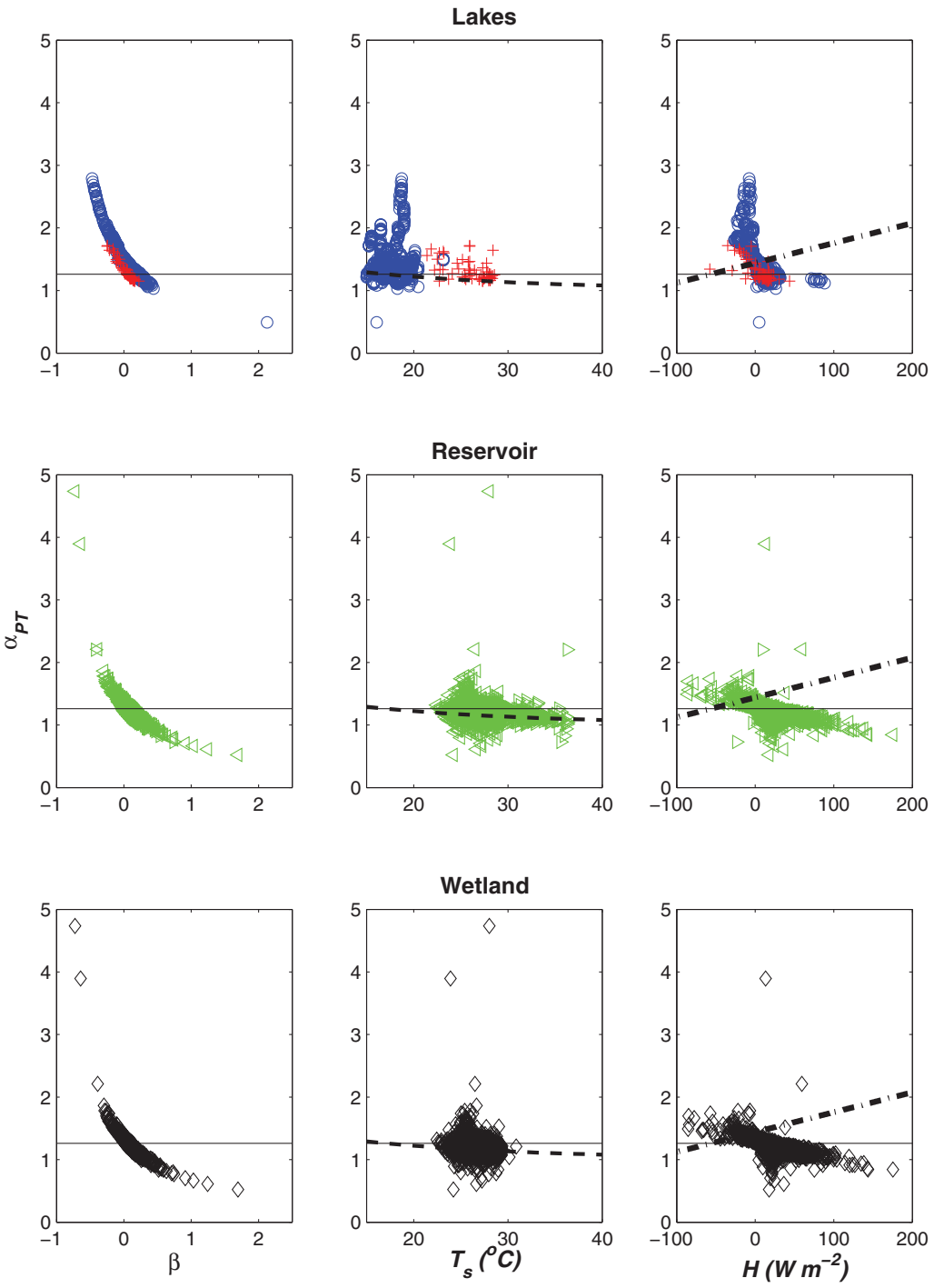

Figure 2. Variations of the Priestley-Taylor coefficient α_{PT} across the sites labeled as *Lakes* with Lake Léman in circle (o) and Lake Kinneret in plus (+), *Reservoirs* with the settling reservoir in greater than symbol (>) and the operational reservoir in less than symbol (<), and *Wetland* in diamond (◇) with (left) measured Bowen ratio β, (middle) measured surface temperature T_s, and (right) measured sensible heat flux H. The α_{avg} predicted from equation (5) is shown in all the middle plots (dashed), and the relation between α_{PT} and H derived over crops as described elsewhere [*Pereira and Villa-Nova*, 1992] is also shown in the right plots (dash-dot). $\alpha_{PT} = 1.26$ is also shown as a thin-horizontal line.

β is not necessarily universal across data sets, which was also found by *Guo et al.* [2015]. This is due to the role of $(\Delta+\gamma)/\Delta$, which is primarily dependent on T_s. The largest α_{PT} corresponds to the most negative β due to advection, as expected from the definition in equation (6). Again, the presentation of $\alpha_{PT}-\beta$ in

Figure 2 (left) should not be interpreted as model-data comparisons. It simply highlights the ranges of α_{PT} and β covered at each of the sites.

Whether these α_{PT} variations over water can be entirely explained by T_s changes as conjectured from equation (5) or H as proposed by a previous study over crops [*Pereira and Villa-Nova*, 1992] is now considered. The relation between computed α_{PT} values from equation (6) and T_s (middle) or H (right) for data corresponding to different water bodies is also presented in Figure 2. The horizontal thin line shows the widely used $\alpha_{PT} = 1.26$. It appears that there are no significant trends between measured α_{PT} and T_s above water surfaces. In several sites, and especially in the wetland, most of the α_{PT} values are subunity. Figure 2 also shows variations in α_{avg} computed from equation (5) with measured T_s (i.e., dashed lines in the middle plots), suggesting that surface temperature alone introduces large deviations from the accepted 1.26 value. In fact, the α_{avg} variations in Figure 2 span a portion of the variations reported over water surfaces, although large scatter has already been reported in many studies depending on local conditions [*Szilagyi et al*., 2014].

Regarding the relation between α_{PT} and H, this relation appears to be stronger than its T_s counterpart with α_{PT} decreasing as H increases. The shape of the α_{PT}-H relation seems to depend on the nature of the water body and is clearly not universal. Lake Léman and the wetland site do not follow a linear relation across the entire range of measured H as found for Lake Kinneret and the Eshkol reservoirs. Evidently, measured H alone also cannot explain the entire scatter in measured α_{PT} between or across sites. However, $\alpha_{PT} > 1.26$ appears to be associated with $H < 0$ while $\alpha_{PT} < 1.26$ appears to be associated with $H > 0$, with large scatter in α_{PT} occurring when $H \approx 0$ both for Lake Léman and the Tilopozo wetland. Interestingly, the general trend of α_{PT} decreasing with increasing H in Figure 2 is opposite to a linear increase in α_{PT} with increasing H reported for crops [*Pereira and Villa-Nova*, 1992]. What causes the difference in the α_{PT}-H relation for free water surfaces and crops remains unclear. Some studies over well-watered crops also suggest a trend consistent with the free water surfaces here. For example, it was found by *Jury and Tanner* [1975] that for several well-irrigated crops, horizontal advection of dry air mass causes daily α_{PT} to increase beyond its value inferred from measurements on nonadvective days as expected. The values of H inferred by us from the *Jury and Tanner* [1975] study suggest that $H < 0$ during those advective conditions, which is in line with the free water surface data results here. An empirical correction based on vapor pressure deficit to α_{PT} in the aforementioned study appears to improve the agreement between model calculations and lysimeter measurements of E. However, it is clear that the α_{PT} variations above water surfaces cannot be fully explained by T_s or H variations.

The prediction of α_{PT} variations from routine meteorological measurements using the flux-variance method is now discussed. Routine meteorological instruments for air temperature (e.g., thermocouples) and water vapor (e.g., hygrometers using electric capacitive elements) are slow-response instruments and are commonly sampled at 0.1–1 Hz. Hence, prior to any discussion on α_{PT} variability, it is necessary to assess how well R_{wT}/R_{wq} and R_{Tq} can be inferred from filtered and down-sampled time series. To do so, numerical experiments are conducted on the 20 Hz (i.e., the highest sampling frequency across all experiments) temperature and water vapor series collected above Lake Léman (in Switzerland), as a case study. To mimic various types of instrumentation filtering and subsampling and yet maintain some generality without imposing "instrument specific" filtering, one-dimensional Gaussian and box filter functions are applied to the 20 Hz series for conducting "low-pass" filtering (i.e., high frequencies filtered but low frequencies retained). The filtered series of some arbitrary flow variable S (i.e., w', q', or T'), denoted as $\tilde{S}$, is computed from the convolution

$$\tilde{S} = \int_{-\infty}^{\infty} G(r) S(t-r) dr, \tag{16}$$

where t denotes time and $G(r)$ is a filter function. The Gaussian filter function is a Gaussian distribution with mean zero and variance set to $(1/12)\delta^2$, where δ is the cutoff frequency [*Pope*, 2000]. Similar filter function can be derived for box filtering as discussed elsewhere [*Pope*, 2000]. Figure 3 shows an example of how a 20 Hz time series of w', q', and T' is filtered to 0.1 Hz using a one-dimensional Gaussian $G(r)$. The example in Figure 3 corresponds to the case with $H = 75$ Wm^{-2}, $E = 217$ W m^{-2}, $\alpha_{PT} = 0.74$, and $T_s = 18.1$°C, which yields $R_{wT}/R_{wq} = 1.01$, $R_{\tilde{w}\tilde{T}}/R_{\tilde{w}\tilde{q}} = 1.06$, $R_{Tq} = 0.86$, and $R_{\tilde{T}\tilde{q}} = 0.83$.

Figure 4 shows comparisons between R_{wT}/R_{wq} measured at 20 Hz against R_{wT}/R_{wq} determined by applying a Gaussian $G(r)$ to w', T', and q'. Three cutoff frequencies for $G(r)$ are selected as 2, 1, and 0.1 Hz to illustrate

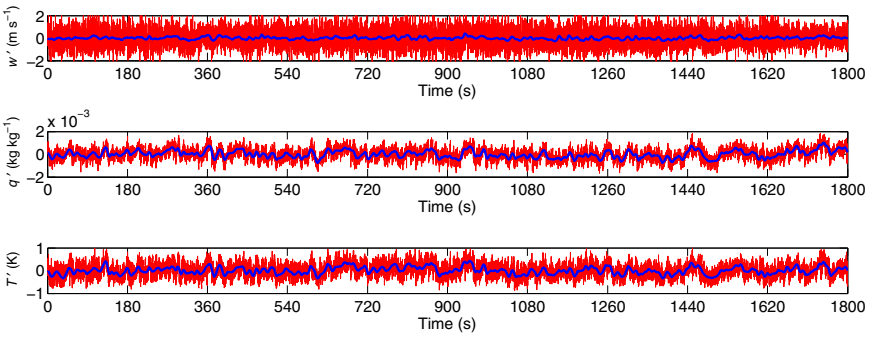

Figure 3. The 20 Hz (red) and filtered (blue, with a cutoff frequency of 0.1 Hz) w', q', and T' over a 30 min segment collected above Lake Léman, which are used to assess how well T_r can be inferred from R_{Tq} when the sampling frequency is degraded and the averaging window is increased using Gaussian filtering.

how progressive degradation in sampling and increased filtering affects T_r. The results obtained using the box filter function are almost identical to those obtained using the Gaussian filter function and are thus not shown for brevity (but do suggest that the findings here are not sensitive to the precise filtering mechanism by the instruments). The main finding from Figure 4 is that individually, the 20 Hz measured R_{wT}/R_{wq} and R_{Tq} terms in equation (11) can be reasonably determined from filtered series even when the cutoff frequency is as low as 0.1 Hz. The R^2 values are slightly reduced as the cutoff frequency is reduced, which is consistent with previous studies showing that increased filtering does not change flux estimates but increases the scatter [*Bosveld and Beljaars*, 2001; *Tanny et al*., 2010].

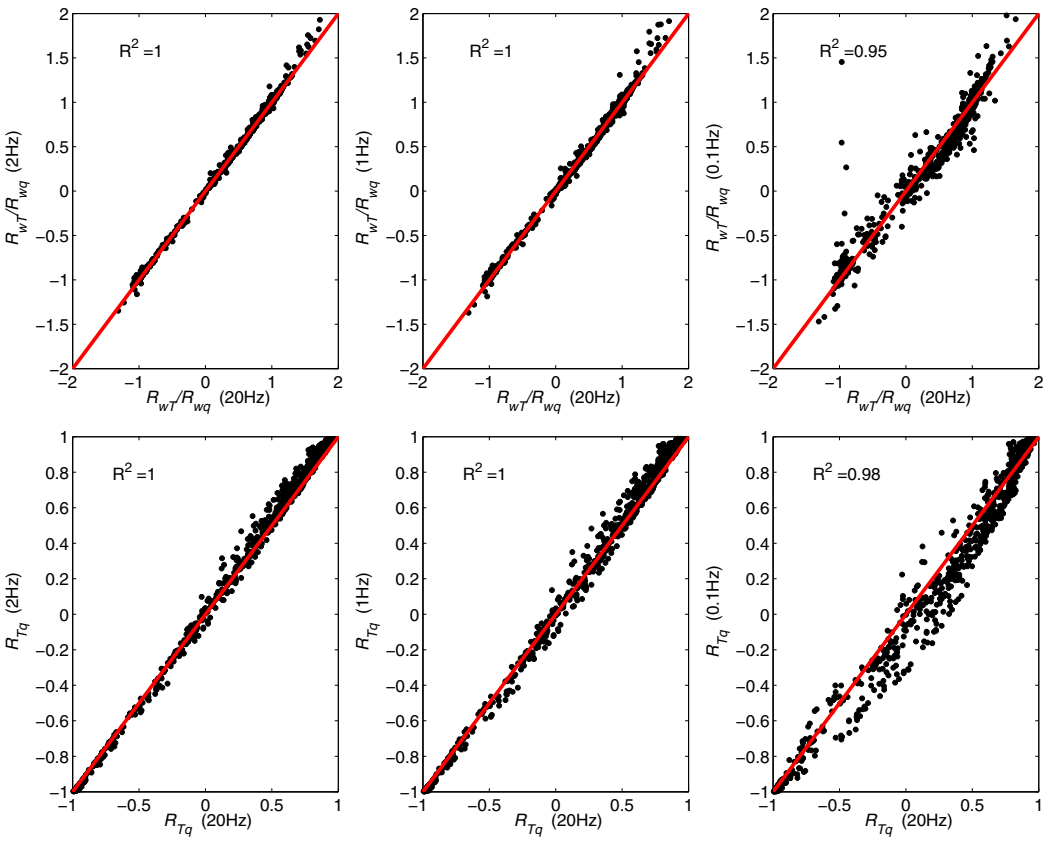

Figure 4. Estimation of R_{wT}/R_{wq} and R_{Tq} at different cutoff frequencies using data from Lake Léman. The T', q', and w' series are Gaussian filtered at preset cutoff frequencies, and R_{wT}/R_{wq} as well as R_{Tq} are recomputed and compared to those sampled at the highest sampling frequency (=20Hz). R^2 values are also shown.

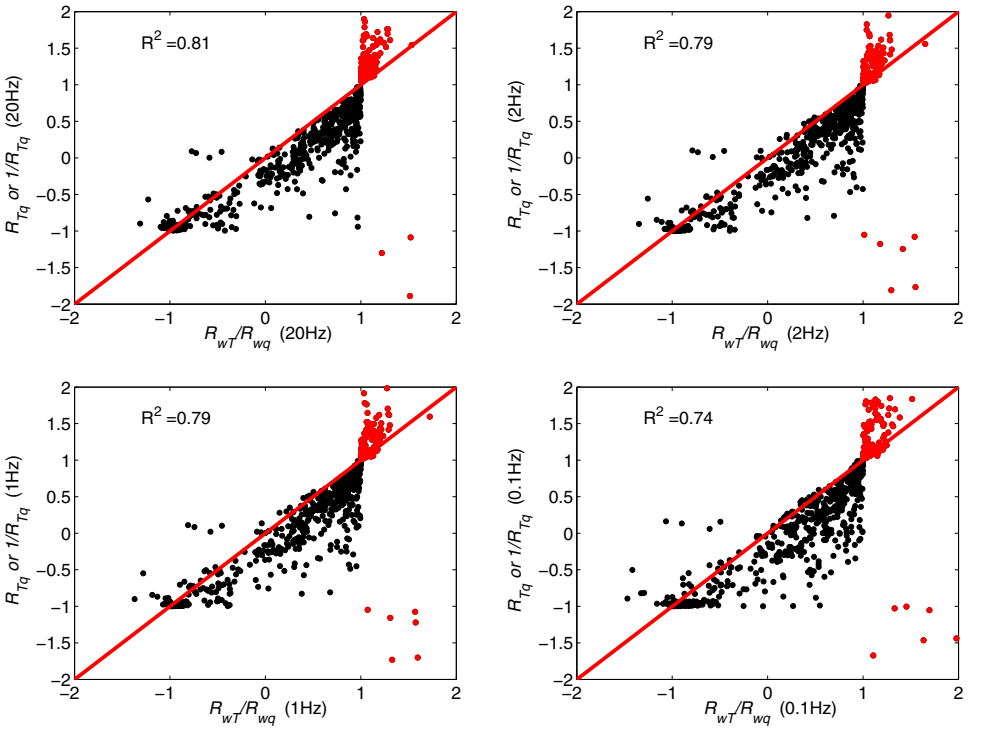

Figure 5. Estimation of relative transport efficiency $T_r = R_{wT}/R_{wq}$ from R_{Tq} or R_{Tq}^{-1} at different cutoff frequencies using data from Lake Léman as illustration. The comparisons are shown across various cutoff frequencies. The one-to-one line is shown for reference. The agreement suggests that $T_r = R_{wT}/R_{wq}$ can be determined from R_{Tq} or R_{Tq}^{-1} even when the cutoff frequency of 0.1 Hz is reached. Red color is for $R_{wT}/R_{wq} > 1$ and black color is for $R_{wT}/R_{wq} < 1$. R^2 values are also shown.

Figure 5 presents the comparison between measured R_{wT}/R_{wq} and T_r modeled by equation (11) (i.e., $= R_{Tq}$ or R_{Tq}^{-1}) using data collected above Lake Léman. Here R_{wT}/R_{wq} and R_{Tq} are again compared for various subsampling and filtering cutoff frequencies. It can be surmised from the comparison in Figure 5 that the estimation of T_r from R_{Tq} or R_{Tq}^{-1} appears to be reasonable even when a cutoff frequency of 0.1 Hz is reached. Similar results were found using data collected over the Eshkol reservoirs (not shown for brevity).

Modeled α_{PT} using equation (15) with $T_r = R_{wT}/R_{wq}$ (top) and $T_r = R_{Tq}$ or R_{Tq}^{-1} (bottom) plots are compared to measured α_{PT} using data collected over both Lake Léman and the Eshkol reservoirs as shown in Figure 6. Comparisons are repeated across several cutoff frequencies and are all referenced to the α_{PT} determined by the 20 Hz lake (or 10 Hz for the Eshkol reservoirs) data. Good agreement between measured and modeled α_{PT} is maintained when $T_r = R_{wT}/R_{wq}$ is directly used even for a cutoff frequency of 0.1 Hz. Acceptable agreement between measured and modeled α_{PT} is also observed when $T_r = R_{Tq}$ or R_{Tq}^{-1} is employed for a cutoff frequency of 0.1 Hz, which suggests that equation (15) can be confidently used even when measurements of T' and q' are filtered and subsampled to 0.1 Hz.

For practical applications, it remains challenging to a priori determine whether R_{Tq} or R_{Tq}^{-1} should be used for T_r without any information about the vertical velocity. Previous studies have shown that R_{Tq} is a better surrogate for R_{wT}/R_{wq} over wet surfaces where the transport efficiency of water vapor (R_{wq}) is usually higher than that of heat (R_{wT}) [*Bink and Meesters*, 1997]. Guided by this finding, Figure 7 shows a comparison between α_{PT} determined using equation (15) with $T_r = R_{Tq}$ and measured α_{PT} using data collected over both Lake Léman and the Eshkol reservoirs. It is clear that the modeled α_{PT} with $T_r = R_{Tq}$ at different cutoff frequencies (2, 1, and 0.1 Hz) all agree with the calculated α_{PT} using the 20 Hz lake (or 10 Hz for the Eshkol reservoirs) data. Interestingly, the R^2 values appear to be higher than those in Figure 6 where a distinction in $T_r = R_{Tq}$ or R_{Tq}^{-1} is employed. This finding suggests that setting $T_r = R_{Tq}$ may be sufficient for operationally determining α_{PT} above wet surfaces in the absence of any other information. Modeled α_{PT} with $T_r = 1/R_{Tq}$ in equation (15) is also compared to the calculated α_{PT}. Results (not shown here) indicate that using $T_r = 1/R_{Tq}$ yields a worse outcome when compared to setting $T_r = R_{Tq}$.

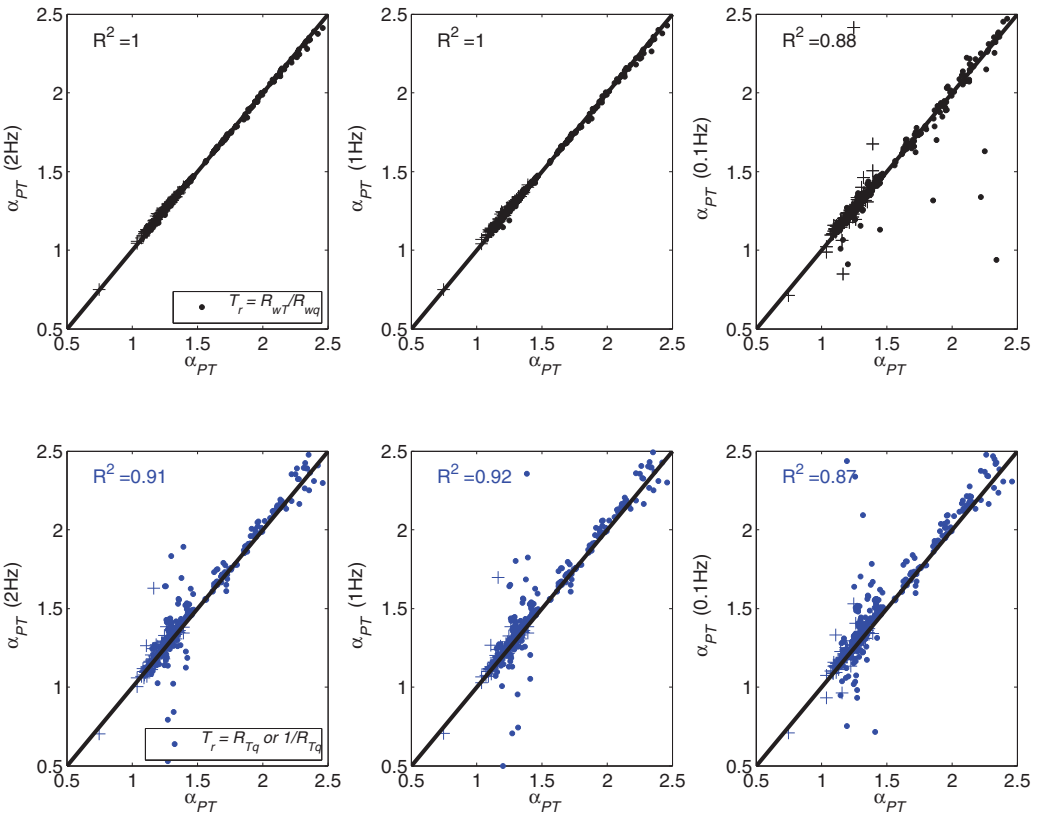

Figure 6. Estimation of α_{PT} using equation (15) with (top) $T_r = R_{wT}/R_{wq}$ and (bottom) $T_r = R_{Tq}$ or R_{Tq}^{-1} using data from Lake Léman (circles) and the Eshkol reservoirs (pluses). Comparisons are shown across various reduced cutoff frequencies (2, 1, and 0.1 Hz—left to right) referenced to 20 Hz (or 10 Hz for the Eshkol reservoirs). The *x* axes are all calculated at 20 Hz (or 10 Hz for the Eshkol reservoirs) using equation (10). The *y* axes are calculated at the various cutoff frequencies using equation (15) with two different transfer coefficients ((top) $T_r = R_{wT}/R_{wq}$ and (bottom) $T_r = R_{Tq}$ or R_{Tq}^{-1}). The good agreement (see the R^2 values) between measured and modeled α_{PT} when $T_r = R_{wT}/R_{wq}$ is used is featured in the top plots and the acceptable agreement when $T_r = R_{Tq}$ or R_{Tq}^{-1} is employed is featured in the bottom plots. These findings suggest that equation (15) can be employed even when measurements of T' and q' are filtered and subsampled to 0.1 Hz.

Further analysis is now conducted on equation (15) to assess whether α_{PT} is sensitive to the ratio σ_T/σ_q or R_{Tq} or both and also to offer a conjecture as to why setting $T_r = R_{Tq}$ provides reasonable estimates of α_{PT} (see Figure 7) over water surfaces. Figure 8 shows that, to a first order, R_{Tq} appears to explain much of the variability in α_{PT} (at

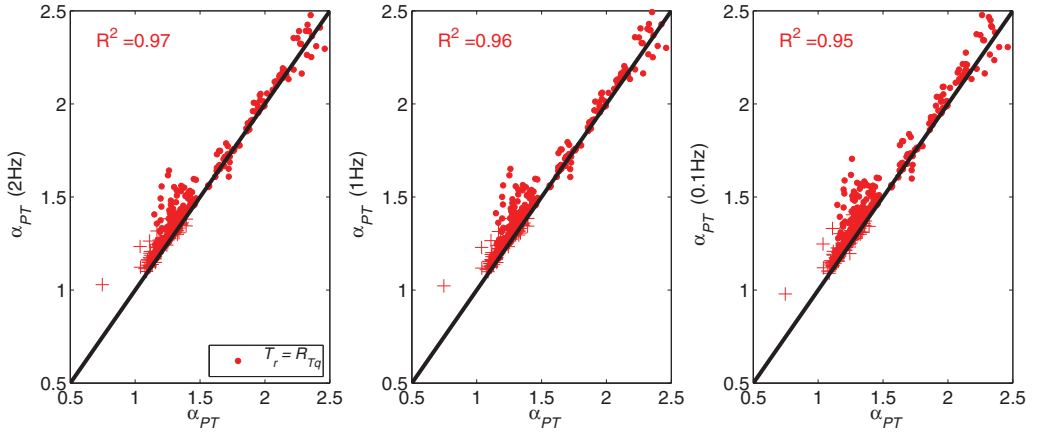

Figure 7. Estimation of α_{PT} using equation (15) with $T_r = R_{Tq}$ using data from Lake Léman (circles) and the Eshkol reservoirs (pluses). Comparisons are shown across various reduced cutoff frequencies referenced to the 20 Hz (or 10 Hz for the Eshkol reservoirs). The *x* axes are all calculated at 20 Hz (or 10 Hz for the Eshkol reservoirs) using equation (10). The *y* axes are calculated at different cutoff frequencies using equation (15) with $T_r = R_{Tq}$.

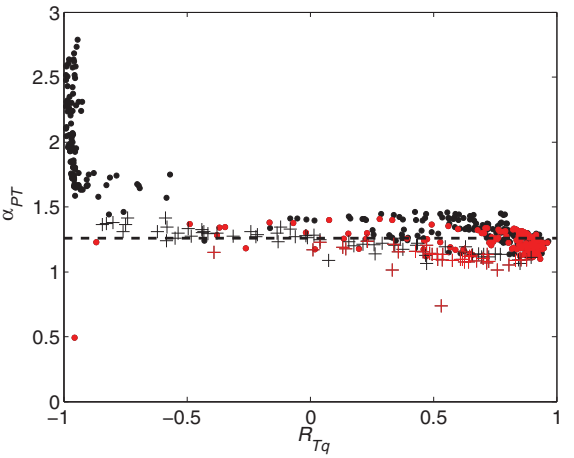

Figure 8. Variations of measured α_{PT} with R_{Tq} using data from Lake Léman (circles) and the Eshkol reservoirs (pluses). Red color is for $R_{wT}/R_{wq} > 1$ and black color is for $R_{wT}/R_{wq} < 1$.

least for Lake Léman and Eshkol reservoirs) provided $R_{Tq} > -0.9$. This suggests that setting $T_r = R_{Tq}$ yields the best estimates over water surfaces as the prevalence of $R_{Tq} < -0.9$ appears to be rare. As $R_{Tq} \to -1$, α_{PT} increases rapidly above its accepted 1.26 value. In this limit, the energy for evaporation is likely to be provided by downwind advected sensible heat flux, with zero net available energy. As a result, and according to equation (6), $\beta \to -1$ and $\alpha_{PT} \to \infty$. However, as $R_{Tq} \to +1$, α_{PT} gradually decreases to values below 1.26.

Given this theoretical (i.e., equation (15)) and empirical (i.e., Figure 8) connection between α_{PT} and R_{Tq}, as well as the connection between R_{Tq} and advection/entrainment processes [*De Bruin et al.*, 1999; *Katul et al.*, 2008; *Moene and Schüttemeyer*, 2008; *Li et al.*, 2012a], a number of observations can now be made. During strong horizontal advective conditions of dry air, when $R_{Tq} \to -1$, it is expected that $\alpha_{PT} > 1.26$, which is consistent with advection studies reported over well-irrigated crops. Likewise, if the entrainment process at the top of the atmospheric boundary layer affects the surface fluxes, α_{PT} also becomes larger than 1.26 since entrainment is associated with strongly negative R_{Tq}. When neither advection nor entrainment processes are prominent, and sources and sinks of heat and water vapor at the surface are quite similar, $R_{Tq} \to +1$. Under such conditions, α_{PT} is around but can drop below its accepted 1.26 value.

5. Conclusions

Variability in the Priestley-Taylor (PT) coefficient α_{PT} was analyzed at subdaily time scales over large lakes, reservoirs, and wetlands that feature wide variations in water body sizes and climatic conditions. It was shown that neither surface water temperature nor measured sensible heat flux variations explain the deviations in α_{PT} from its accepted 1.26 value over water surfaces for almost all cases considered. The relative transport efficiency of turbulent heat and water vapor is key to explaining the variability in α_{PT}. A new method that allows the determination of α_{PT} operationally using standard meteorological sensors is proposed and tested. The proposed method explains much of the measured variations in α_{PT} even when different filtering schemes and cutoff frequencies (as low as 0.1 Hz) are used to represent instrument filtering and subsampling. A consequence of this finding is a recommendation to compute R_{Tq} in experiments even when slow-response sensors are deployed as this quantity may be used to assess variability in α_{PT} over water surfaces. The performance of this method over land is an interesting question for future research. The broader impact of this work is its capability to estimate diurnal variations of the evaporative fraction from routine meteorological data, which can then be used to infer sensible and latent heat fluxes from remote sensing measurements. The evaporative fraction $EF = E/(R_n - G)$, routinely used in up-scaling remote sensing measurements in time [*Anderson et al.*, 2008], can be directly linked to α_{PT} using $\alpha_{PT} = EF(1 + \gamma/\Delta)$. Hence, the work here (e.g., equation (15)) directly benefits such up-scaling efforts by allowing EF to evolve during the day based on routine meteorological measurements. Another utility of this work is a potential link between K_T/K_q deviations from unity (as in equation (9)) and T_r (= R_{Tq} or R_{Tq}^{-1} as in equation (15)), where T_r again can be inferred from filtered and low-frequency measurements.

Acknowledgments

D.L. acknowledges support from the NOAA (U.S. Department of Commerce) grant NA08OAR4320752 and the Carbon Mitigation Initiative at Princeton University, sponsored by BP. The statements, findings, and conclusions are those of the authors and do not necessarily reflect the views of the NOAA, the U.S. Department of Commerce, or BP. G.K. acknowledges support from the National Science Foundation (NSF-EAR-1344703, NSF-AGS-1102227, and NSF-CBET-103347), the United States Department of Agriculture (2011-67003-30222), the U.S. Department of Energy (DOE) through the office of Biological and Environmental Research (BER) Terrestrial Ecosystem Science (TES) Program (DE-SC0006967 and DE-SC0011461), and the Binational Agricultural Research and Development (BARD) Fund (IS-4374-11C). The data used in this study are available from the corresponding author upon request.

References

Aminzadeh, M., and D. Or (2014), Energy partitioning dynamics of drying terrestrial surfaces, *J. Hydrol.*, *519*, 1257–1270, doi:10.1016/j.jhydrol.2014.08.037.

Anderson, M., J. Norman, W. Kustas, R. Houborg, P. Starks, and N. Agam (2008), A thermal-based remote sensing technique for routine mapping of land-surface carbon, water and energy fluxes from field to regional scales, *Remote Sens. Environ.*, *112*(12), 4227–4241, doi:10.1016/j.rse.2008.07.009.

Assouline, S., and Y. Mahrer (1993), Evaporation from Lake Kinneret: 1. Eddy correlation measurements and energy budget estimate, *Water Resour. Res.*, *29*, 901–910.

Assouline, S., S. Tyler, J. Tanny, S. Cohen, E. Bou-Zeid, M. Parlange, and G. Katul (2008), Evaporation from three water bodies of different sizes and climates: Measurements and scaling analysis, *Adv. Water Resour.*, *31*(1), 160–172, doi:10.1016/j.advwatres.2007.07.003.
Bates, G. T., S. W. Hostetler, and F. Giorgi (1995), Two-year simulation of the great lakes region with a coupled modeling system, *Mon. Weather Rev.*, *123*(5), 1505–1522.
Bink, N., and A. Meesters (1997), Comment on estimation of surface heat and momentum fluxes using the flux-variance method above uniform and non-uniform terrain by Katul et al. (1995), *Boundary Layer Meteorol.*, *84*(3), 497–502.
Blanken, P. D., W. R. Rouse, A. D. Culf, C. Spence, L. D. Boudreau, J. N. Jasper, B. Kochtubajda, W. M. Schertzer, P. Marsh, and D. Verseghy (2000), Eddy covariance measurements of evaporation from great slave lake, northwest territories, Canada, *Water Resour. Res.*, *36*, 1069–1077.
Blanken, P. D., W. R. Rouse, and W. M. Schertzer (2003), Enhancement of evaporation from a large northern lake by the entrainment of warm, dry air, *J. Hydrometeorol.*, *4*(4), 680–693.
Blanken, P. D., C. Spence, N. Hedstrom, and J. D. Lenters (2011), Evaporation from lake superior: 1. Physical controls and processes, *J. Great Lakes Res.*, *37*(4), 707–716.
Bosveld, F. C., and A. C. Beljaars (2001), The impact of sampling rate on eddy-covariance flux estimates, *Agric. For. Meteorol.*, *109*(1), 39–45.
Bou-Zeid, E., N. Vercauteren, M. B. Parlange, and C. Meneveau (2008), Scale dependence of subgrid-scale model coefficients: An a priori study, *Phys. Fluids*, *20*(11), 115–106.
Brutsaert, W. (2005), *Hydrology: An Introduction*, Cambridge Univ. Press, N. Y.
Brutsaert, W., and H. Stricker (1979), An advection-aridity approach to estimate actual regional evapotranspiration, *Water Resour. Res.*, *15*, 443–450, doi:10.1029/WR015i002p00443.
Chen, D., and W. Brutsaert (1995), Diagnostics of land surface spatial variability and water vapor flux, *J. Geophys. Res.*, *100*, 25,595–25,606, doi:10.1029/95JD00973.
Cho, J., T. Oki, P.-F. Yeh, W. Kim, S. Kanae, and K. Otsuki (2012), On the relationship between the Bowen ratio and the near-surface air temperature, *Theor. Appl. Climatol.*, *108*(1–2), 135–145, doi:10.1007/s00704-011-0520-y.
Courant, R., and D. Hilbert (1953), *Methods of Mathematical Physics*, vol.1, John Wiley, N. Y.
Crago, R., and R. Crowley (2005), Complementary relationships for near-instantaneous evaporation, *J. Hydrol.*, *300*, 199–211, doi:10.1016/j.jhydrol.2004.06.002.
Crago, R. D. (1996), Comparison of the evaporative fraction and the Priestley-Taylor α for parameterizing daytime evaporation, *Water Resour. Res.*, *32*, 1403–1409.
Culf, A. (1994), Equilibrium evaporation beneath a growing convective boundary layer, *Boundary Layer Meteorol.*, *70*(1-2), 37–49, doi:10.1007/BF00712522.
Davis, J., and C. Allen (1973), Equilibrium, potential and actual evaporation from cropped surfaces in southern Ontario, *J. Appl. Meteorol.*, *12*, 649–657.
De Bruin, H. (1983), A model of the Priestley-Taylor parameter α, *J. Clim. Appl. Meteorol.*, *22*, 572–578.
De Bruin, H., and J. Keijman (1979), The Priestley-Taylor evaporation model applied to a large, shallow lake in the Netherlands, *J. Appl. Meteorol.*, *18*, 898–903.
De Bruin, H., B. Van Den Hurk, and L. Kroon (1999), On the temperature-humidity correlation and similarity, *Boundary Layer Meteorol.*, *93*(3), 453–468.
Eichinger, W. E., M. B. Parlange, and H. Stricker (1996), On the concept of equilibrium evaporation and the value of the Priestley-Taylor coefficient, *Water Resour. Res.*, *32*, 161–164, doi:10.1029/95WR02920.
Flint, A. L., and S. W. Childs (1991), Use of the Priestley-Taylor evaporation equation for soil water limited conditions in a small forest clearcut, *Agric. For. Meteorol.*, *56*, 247–260, doi:10.1016/0168-1923(91)90094-7.
Granger, R. (1989), A complementary relationship approach for evaporation from nonsaturated surfaces, *J. Hydrol.*, *111*(1–4), 31–38, doi:10.1016/0022-1694(89)90250-3.
Granger, R., and D. Gray (1989), Evaporation from natural nonsaturated surfaces, *J. Hydrol.*, *111*(1–4), 21–29, doi:10.1016/0022-1694(89)90249-7.
Granger, R., and N. Hedstrom (2011), Modelling hourly rates of evaporation from small lakes, *Hydrol. Earth Syst. Sci.*, *15*(1), 267–277.
Guo, X., H. Liu, and K. Yang (2015), On the application of the Priestley–Taylor relation on sub-daily time scales, *Boundary Layer Meteorol.*, *156*, 489–499.
Huntingford, C., and J. Monteith (1998), The behaviour of a mixed-layer model of the convective boundary layer coupled to a big leaf model of surface energy partitioning, *Boundary Layer Meteorol.*, *88*(1), 87–101.
Jarvis, P. G., and K. McNaughton (1986), Stomatal control of transpiration: Scaling up from leaf to region, *Adv. Ecol. Res.*, *15*, 1–49.
Jonsson, A., J. Åberg, A. Lindroth, and M. Jansson (2008), Gas transfer rate and CO_2 flux between an unproductive lake and the atmosphere in northern Sweden, *J. Geophys. Res.*, *113*, G04006, doi:10.1029/2008JG000688.
Jury, W., and C. Tanner (1975), Advection modification of the Priestley and Taylor evapotranspiration formula, *Agron. J.*, *67*, 840–842, doi:10.2134/agronj1975.00021962006700060031x.
Katul, G., and C.-I. Hsieh (1997), Reply to the comment by bink and meesters, *Boundary Layer Meteorol.*, *84*(3), 503–509.
Katul, G. G., and C.-I. Hsieh (1999), A note on the flux-variance similarity relationships for heat and water vapour in the unstable atmospheric surface layer, *Boundary Layer Meteorol.*, *90*(2), 327–338.
Katul, G. G., and M. B. Parlange (1992), A Penman-Brutsaert model for wet surface evaporation, *Water Resour. Res.*, *28*, 121–126, doi:10.1029/91WR02324.
Katul, G. G., A. M. Sempreviva, and D. Cava (2008), The temperature–humidity covariance in the marine surface layer: A one-dimensional analytical model, *Boundary Layer Meteorol.*, *126*(2), 263–278.
Komatsu, H. (2005), Forest categorization according to dry-canopy evaporation rates in the growing season: Comparison of the Priestley–Taylor coefficient values from various observation sites, *Hydrol. Processes*, *19*(19), 3873–3896.
Lamaud, E., and M. Irvine (2006), Temperature–humidity dissimilarity and heat-to-water-vapour transport efficiency above and within a pine forest canopy: The role of the Bowen ratio, *Boundary Layer Meteorol.*, *120*(1), 87–109.
Lhomme, J.-P. (1997), A theoretical basis for the Priestley-Taylor coefficient, *Boundary Layer Meteorol.*, *82*(2), 179–191, doi:10.1023/A:1000281114105.
Li, D., and E. Bou-Zeid (2011), Coherent structures and the dissimilarity of turbulent transport of momentum and scalars in the unstable atmospheric surface layer, *Boundary Layer Meteorol.*, *140*(2), 243–262.
Li, D., E. Bou-Zeid, and H. de Bruin (2012a), Monin-Obukhov similarity functions for the structure parameters of temperature and humidity, *Boundary Layer Meteorol.*, *145*(1), 45–67.

Li, D., G. Katul, and E. Bou-Zeid (2012b), Mean velocity and temperature profiles in a sheared diabatic turbulent boundary layer, *Phys. Fluids*, *24*(10), 105105.
Li, D., G. G. Katul, and E. Bou-Zeid (2015), Turbulent energy spectra and cospectra of momentum and heat fluxes in the stable atmospheric surface layer, *Boundary Layer Meteorol.*, *157*, 1–21.
Liu, H., Y. Zhang, S. Liu, H. Jiang, L. Sheng, and Q. L. Williams (2009), Eddy covariance measurements of surface energy budget and evaporation in a cool season over southern open water in Mississippi, *J. Geophys. Res.*, *114*, D04110, doi:10.1029/2008JD010891.
McNaughton, K., and P. Jarvis (1991), Effects of spatial scale on stomatal control of transpiration, *Agric. For. Meteorol.*, *54*(2), 279–302.
McNaughton, K., and T. Spriggs (1986), A mixed-layer model for regional evaporation, *Boundary Layer Meteorol.*, *34*(3), 243–262.
Moene, A. F., and D. Schüttemeyer (2008), The effect of surface heterogeneity on the temperature–humidity correlation and the relative transport efficiency, *Boundary Layer Meteorol.*, *129*(1), 99–113.
Monteith, J. (1995), A reinterpretation of stomatal responses to humidity, *Plant Cell Environ.*, *18*(4), 357–364.
Monteith, J. L. (1981), Evaporation and surface temperature, *Q. J. R. Meteorol. Soc.*, *107*(451), 1–27, doi:10.1002/qj.49710745102.
Nordbo, A., S. Launiainen, I. Mammarella, M. Leppäranta, J. Huotari, A. Ojala, and T. Vesala (2011), Long-term energy flux measurements and energy balance over a small boreal lake using eddy covariance technique, *J. Geophys. Res.*, *116*, D02119, doi:10.1029/2010JD014542.
Nullet, D., and T. W. Giambelluca (1990), Winter evaporation on a mountain slope, Hawaii, *J. Hydrol.*, *112*(3), 257–265.
Panin, G. N., A. Nasonov, T. Foken, and H. Lohse (2006), On the parameterisation of evaporation and sensible heat exchange for shallow lakes, *Theor. Appl. Climatol.*, *85*(3-4), 123–129.
Parlange, M. B., and G. G. Katul (1992a), An advection-aridity evaporation model, *Water Resour. Res.*, *28*, 127–132, doi:10.1029/91WR02482.
Parlange, M. B., and G. G. Katul (1992b), Estimation of the diurnal variation of potential evaporation from a wet bare soil surface, *J. Hydrol.*, *132*(1), 71–89.
Penman, H. L. (1948), Natural evaporation from open water, bare soil and grass, *Proc. R. Soc. London, Ser. A*, *193*(1032), 120–145, doi:10.1098/rspa.1948.0037.
Pereira, A. R. (2004), The Priestley-Taylor parameter and the decoupling factor for estimating reference evapotranspiration, *Agric. For. Meteorol.*, *125*, 305–313, doi:10.1016/j.agrformet.2004.04.002.
Pereira, A. R., and N. A. Villa-Nova (1992), Analysis of the Priestley-Taylor parameter, *Agric. For. Meteorol.*, *61*, 1–9, doi:10.1016/0168-1923(92)90021-U.
Pope, S. (2000), *Turbulent Flows*, 771 pp., Cambridge Univ. Press, Cambridge, U. K.
Priestley, C., and R. Taylor (1972), On the assessment of surface heat flux and evaporation, *Mon. Weather Rev.*, *106*, 81–92.
Rouse, W. R., P. D. Blanken, N. Bussières, A. E. Walker, C. J. Oswald, W. M. Schertzer, and C. Spence (2008), An investigation of the thermal and energy balance regimes of great slave and great bear lakes, *J. Hydrometeorol.*, *9*(6), 1318–1333.
Slatyer, R., and I. McIlroy (1967), *Practical Microclimatology*, Commonw. Sci. Ind. Res. Organ., Melbourne, Australia.
Spittlehouse, D. L., and T. A. Black (1981), A growing season water balance model applied to two douglas fir stands, *Water Resour. Res.*, *17*, 1651–1656, doi:10.1029/WR017i006p01651.
Stannard, D. I. (1993), Comparison of Penman-Monteith, Shuttleworth-Wallace, and modified Priestley-Taylor evapotranspiration models for wildland vegetation in semiarid rangeland, *Water Resour. Res.*, *29*, 1379–1392.
Stannard, D. I., and D. O. Rosenberry (1991), A comparison of short-term measurements of lake evaporation using eddy correlation and energy budget methods, *J. Hydrol.*, *122*(1), 15–22, doi:10.1016/0022-1694(91)90168-H.
Stull, R. (1988), *An Introduction to Boundary Layer Meteorology*, Kluwer Acad., Dordrecht, Netherlands.
Sumner, D. M., and J. M. Jacobs (2005), Utility of Penman–Monteith, Priestley–Taylor, reference evapotranspiration, and pan evaporation methods to estimate pasture evapotranspiration, *J. Hydrol.*, *308*(1), 81–104.
Szilagyi, J. (2014), Temperature corrections in the Priestley and Taylor equation of evaporation, *J. Hydrol.*, *519*, 455–464, doi:10.1016/j.jhydrol.2014.07.040.
Szilagyi, J., and J. Jozsa (2008), New findings about the complementary relationship-based evaporation estimation methods, *J. Hydrol.*, *354*, 171–186, doi:10.1016/j.jhydrol.2008.03.008.
Szilagyi, J., and A. Schepers (2014), Coupled heat and vapor transport: The thermostat effect of a freely evaporating land surface, *Geophys. Res. Lett.*, *41*, 435–441, doi:10.1002/2013GL058979.
Szilagyi, J., M. T. Hobbins, and J. Jozsa (2009), Modified advection-aridity model of evapotranspiration, *J. Hydrol. Eng.*, *14*(6), 569–574.
Szilagyi, J., M. B. Parlange, and G. G. Katul (2014), Assessment of the Priestley-Taylor parameter value from era-interim global reanalysis data, *J. Hydrol. Environ. Res.*, *2*(1), 1–7.
Tanner, B., and J. Greene (1989), *Measurement of Sensible Heat and Water Vapor Fluxes Using Eddy Correlation Methods*, Campbell Sci. Inc., Logan, Utah.
Tanny, J., S. Cohen, S. Assouline, F. Lange, A. Grava, D. Berger, B. Teltch, and M. Parlange (2008), Evaporation from a small water reservoir: Direct measurements and estimates, *J. Hydrol.*, *351*(1), 218–229, doi:10.1016/j.jhydrol.2007.12.012.
Tanny, J., U. Dicken, and S. Cohen (2010), Vertical variation in turbulence statistics and energy balance in a banana screenhouse, *Biosyst. Eng.*, *106*(2), 175–187.
Tanny, J., S. Cohen, D. Berger, B. Teltch, Y. Mekhmandarov, M. Bahar, G. Katul, and S. Assouline (2011), Evaporation from a reservoir with fluctuating water level: Correcting for limited fetch, *J. Hydrol.*, *404*, 146–156, doi:10.1016/j.jhydrol.2011.04.025.
Venturini, V., S. Islam, and L. Rodriguez (2008), Estimation of evaporative fraction and evapotranspiration from MODIS products using a complementary based model, *Remote Sens. Environ.*, *112*(1), 132–141, doi:10.1016/j.rse.2007.04.014.
Vercauteren, N., E. Bou-Zeid, M. Parlange, U. Lemmin, H. Huwald, J. Selker, and C. Meneveau (2008), Subgrid-scale dynamics of water vapour, heat, and momentum over a lake, *Boundary Layer Meteorol.*, *128*(2), 205–228, doi:10.1007/s10546-008-9287-9.
Viswanadham, Y., V. S. Filho, and R. Andre (1991), The Priestley-Taylor parameter α for the amazon forest, *For. Ecol. Manage.*, *38*(3), 211–225, doi:10.1016/0378-1127(91)90143-J.
Wang, J., G. D. Salvucci, and R. L. Bras (2004), An extremum principle of evaporation, *Water Resour. Res.*, *40*, W09303, doi:10.1029/2004WR003087.
Yang, H., D. Yang, and Z. Lei (2013), Seasonal variability of the complementary relationship in the Asian monsoon region, *Hydrol. Processes*, *27*(19), 2736–2741, doi:10.1002/hyp.9400.
Yu, T. (1977), Parameterization of surface evaporation rate for use in numerical modeling, *J. Appl. Meteorol.*, *16*, 393–400.